Journal of Structural Geology 33 (2011) 698–712

Contents lists available at ScienceDirect

Journal of Structural Geology

journal homepage: www.elsevier.com/locate/jsg

Grain coarsening in polymineralic contact metamorphic carbonate rocks: The role of different physical interactions during coarsening

Sabine H. Brodhag [a,*], Marco Herwegh [a], Alfons Berger [b]

[a] Institute of Geological Sciences, University of Bern, 3013 Bern, Switzerland
[b] Department of Geography and Geology, University of Copenhagen, Denmark

ARTICLE INFO

Article history:
Received 24 November 2009
Received in revised form
30 November 2010
Accepted 6 December 2010
Available online 21 December 2010

Keywords:
Static grain growth
Calcite
Second-phase particle
Zener pinning
Coupled grain coarsening
Microstructure
Polymineralic
Nearest neighbor

ABSTRACT

The microstructural evolution of polymineralic contact metamorphic calcite marbles (Adamello contact aureole) with variable volume fractions of second-phase minerals were quantitatively analyzed in terms of changes in grain size and nearest neighbor relations, as well as the volume fractions, dispersion and occurrences of the second phases as a function of changing metamorphic conditions. In all samples, the calcite grain size is controlled by pinning of grain boundaries by second phases, which can be expressed by the Zener parameter (Z), i.e., the ratio between size and volume fraction of the second phases. With increasing peak metamorphic temperature, both the sizes of matrix grains and second phases increase in dependence on the second-phase volume fraction. Two distinct coarsening trends are revealed: trend I with coupled grain coarsening limited by the growth of the second phases is either characterized by large-sized or a large number of closely spaced-second phase particles, and results finally in a dramatic increase in the calcite grain size with Z. Trend II is manifest by matrix controlled grain growth, which is retarded by the presence of single second-phase particles that are located on calcite grain boundaries. It is supported by grain boundary pinning induced by triple junctions, and the calcite grain size increases moderately with Z. The two different grain coarsening trends manifest the transition between relatively pure polymineralic aggregates (trend II) and microstructures with considerable second-phase volume fractions of up to 0.5. The variations might be of general validity for any polymineralic rock, which undergoes grain coarsening during metamorphism. The new findings are important for a better understanding of the initiation of strain localization based on the activation of grain size dependent deformation mechanisms.

1. Introduction

The growth of minerals is a fundamental process in all rocks that underwent metamorphism (e.g., Joesten, 1991). Knowledge on the changes in grain size is important, because grain size increases are directly related to changes in the grain boundary network affecting the mass-transfer pathways on the grain-scale, which is relevant for many metamorphic and deformed rocks in the Earth's crust and mantle. Under static conditions, a monomineralic rock increases its grain size continuously, following grain growth kinetics as defined by exponential laws (Simpson et al., 1971; Poirier and Guillopé, 1979; Joesten, 1983, 1991; Olgaard and Evans, 1986). Surface energy is the main driving force for grain growth in such pure aggregates (Evans et al., 2001 and references therein), which might be counteracted, however, by pinning of grain boundaries due to triple junction drag (Shvindlerman and Gottstein, 2005; Piazolo et al., 2006).

In nature, rocks are rarely monomineralic and very small volume fractions of additional minerals, so-called second phases, impose an effect on grain growth of the matrix phase (Riege et al., 1999; Weygand et al., 2000; Berger and Herwegh, 2004; Herwegh and Berger, 2004; Ferry et al., 2005; Zheng et al., 2006). Generally speaking, the mean grain size in a polymineralic aggregate is the time integrated product of the grain coarsening process at elevated temperatures as is the case for contact metamorphism, for example. In order to understand grain coarsening and to predict the evolution of grain sizes in such polymineralic rocks, an understanding of the effect of the second phases on the migrating grain boundaries of the matrix phase is crucial. In this sense, second phases can counteract the surface energy of matrix grains by imposing a dragging force on the migrating grain boundaries, resulting in a retardation of grain growth of the matrix phase (see Fig. 6, Brodhag and Herwegh, 2009) or even in a complete immobilization of the grain boundaries inducing a stabilization of the matrix's grain size. Hence, the second phases can directly control the grain size of the matrix phase. Generally, second phases have to be

* Corresponding author.
E-mail address: brodhag@geo.unibe.ch (S.H. Brodhag).

0191-8141/$ – see front matter © 2010 Elsevier Ltd. All rights reserved.
doi:10.1016/j.jsg.2010.12.003

List of symbols and abbreviations

c	constant in the Zener equation
cc	calcite
CPP	clustered particle pinning
D	mean matrix grain size
D_{cc}	mean calcite matrix grain size
D_{max}	maximum matrix grain size
D_{nor}	mean norcamphor matrix grain size
d_p	mean second-phase grain size
f_p	second-phase volume fraction
gb	grain boundary (of a matrix grain)
K	nearest neighbor correlation parameter
m	parameter assigning the spatial location of second phases
M_{cc}	modes of nearest neighbor distribution of calcites
MPP	multiple particle pinning
M_{sp}	modes of nearest neighbor distribution of second phases
n(cc)	number of calcite grains
n(sp)	number of second-phase particles
sp	second phase
SPP	single particle pinning
t	time
T	temperature
TJP	triple junction pinning
Z	Zener parameter

discriminated into solid and liquid/gaseous second phases as they behave in a rigid and deformable manner respectively during pinning, imposing therefore different physical interactions onto a migration grain boundary (Evans et al., 2001; Petrishcheva and Renner, 2005). For both types the amount, size and dispersion of the second phases define if and how the grain boundaries of a matrix phase are affected. In the case of solid second phases, for example, a large number of nano-scale second phases is required (Herwegh and Kunze, 2002; Berger and Herwegh, 2004; Burhan and Ferry, 2006), while for large second phases (with grain sizes comparable to those of the matrix grains) only a small number of second phases are already sufficient to efficiently control the evolution of the grains of the matrix phase. It is this relation between size (d_p) and volume fraction (f_p) on the one side and the grain size of the matrix phase (D) on the other side, which was discovered by Zener (in Smith, 1948).

$$D = c \cdot \frac{d_p}{f_p} \tag{1}$$

This relation has meanwhile variously been modified to express the effect of second phases in polymineralic materials in the case of material sciences (Gladman, 1966; Hellman and Hillert, 1975; Evans et al., 2001; Brodhag and Herwegh, 2009) and for statically affected or deformed polymineralic rocks in nature (Mas and Crowley, 1996; Berger and Herwegh, 2004; Herwegh et al., 2005; Ebert et al., 2007a,b, 2008; Song and Ree, 2007; Herwegh et al., 2008). In addition to second phases, chemical impurities (e.g., Freund et al., 2001; Nakamura et al., 2005; Shvindlerman and Gottstein, 2005), melt films (Renner et al., 2002; Petrishcheva and Renner, 2005), crystallographic misorientations between adjacent grains (Stöckhert and Duyster, 1999; Kruhl, 2001; Bestmann and Prior, 2003; Wheeler et al., 2003) and grain boundary triple junctions (Pande and Masumura, 2005; Piazolo et al., 2005, 2006; Gottstein et al., 2006) can also affect grain growth in polymineralic rocks. Under the presence of solid state second phases, however, all these additional pinning parameters are of minor importance only, as suggested by Shvindlerman and Gottstein (2005) and experimental results of Brodhag and Herwegh (2009).

The effect of second phases on the growing matrix phase can be reduced to two general behaviors. (i) For low second-phase volume fractions, the matrix grain boundaries are pinned or dragged in the aforementioned manner but pinning by individual particles can be overcome as a function of time or increasing temperature. (ii) In the case of high second-phase volume fractions, a complete immobilization of the matrix grain boundaries by pinning due to the large amount of second-phase particles occurs. In this case, a grain size increase of the matrix phase can only take place when the second phases grow, giving more space to allow simultaneous growth of the matrix grains. This combined growth of matrix and second phase is referred to as coarsening and has been treated by experimental and numerical modeling approaches, where the latter either use the minimization in surface energy (e.g., Solomatov et al., 2002) or reduction in chemical gradients (e.g., Ardell, 1972) as major driving forces. In the case of polymineralic natural rocks, however, very little is known about the two effects of second-phase pinning since systematic studies in rocks showing a large variation in second-phase contents are missing so far. To close this gap, this study investigates a series of contact metamorphic calcite marbles with variable volume fractions of second-phase minerals (f_p of 0.0004 up to 0.5). The advantage of a contact metamorphic field laboratory is the chance to obtain temperature and time-resolved information on the microstructural evolution of polymineralic aggregates. This information is mandatory for the interpretation of metamorphic microstructures. With this perspective, we will discuss the variations in the effect of the second phases on the matrix grain size for different metamorphic temperatures as a function of changes in volume fraction and grain size of second phases as well as their dispersion. We will be able to define two different growth behaviors, which are either controlled by the matrix growth and local pinning of matrix grain boundaries by second phases or by complete pinning of matrix grains by second phases, where the coupled growth of matrix and second-phase grains results in larger grain sizes. As will be demonstrated, this distinction depends on variations in the physical pinning processes and is crucial for the interpretation of the evolution of metamorphic rocks.

2. Geological setting

The field area of this study is located northwest of Verona, northern Italy, close to the intersection between the two major Alpine lineaments, the Tonale and Giudicarie Faults (Fig. 1a). The samples investigated were taken from the Calcare di Angolo formation, a Middle Triassic sediment unit east of the Monte Re di Castello tonalite (Adamello intrusions). After a lagoonal and evaporitic milieu, a fast marine transgression in the Anis induced the deposition of the Calcare di Angolo in the form of dark gray micritic and massive (lower part) to thin bedded (upper part) limestones, which are intercalated with marly layers. In the non-metamorphosed limestones, crinoid columnal plates can be found. Contact metamorphism (Brack, 1983; Riklin, 1983), during the emplacement and cooling of the Monte Re di Castello tonalite transformed the original sediments into gray to white calcite marbles. The Monte Re di Castello tonalite is the oldest intrusion of the Adamello complex with an Eocene-Oligocene age of 42–40 Ma (Hansmann and Oberli, 1991) and consists dominantly of tonalitic to granodioritic rocks. Amphibole-rich gabbros and diorites occur

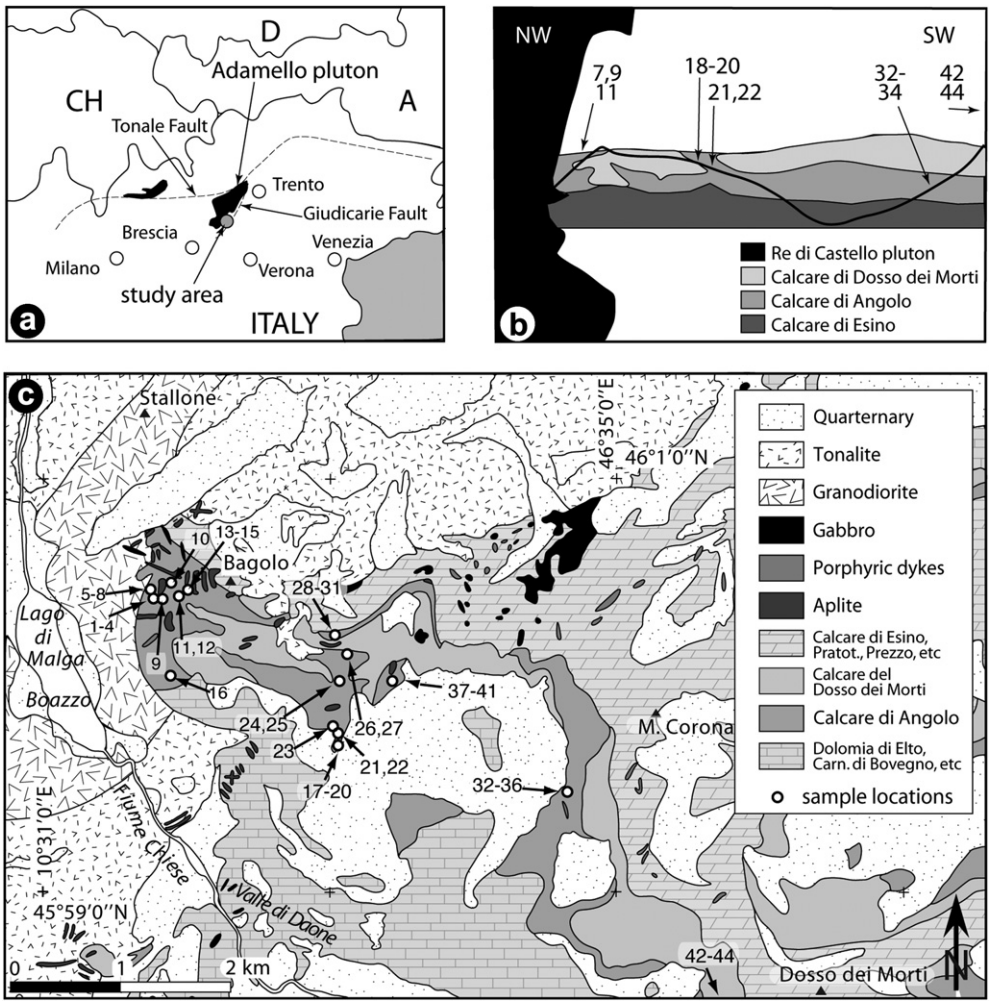

Fig. 1. Locations of study area and samples investigated. a) Location of study area and Adamello pluton (black) in northern Italy (modified after www.maps.google.com). b) Location of samples of the Calcare di Angolo in a projection of a vertical profile, which is oriented perpendicular to the pluton's contact (black). Note that samples SB05-42 and −44 are situated outside the profile and the map (c). c) Geological map of the Valle di Daone area with sample locations. Samples SB05-42 and −44 with a distance of more than 4 km to the pluton contact are not located on the map.

along the contact zone of the batholith (Callegari et al., 1998) and the surrounding rocks are penetrated by swarms of small granite and aplite bodies as well as by lamprophyric dikes (Brack, 1983). The dimension of the metamorphic contact aureole is 1–2 km in maximum and pre-intrusion temperatures for the country rocks were estimated by Riklin (1983) to be at about 200 °C and 600–650 °C and more for maximum peak metamorphic conditions close to the pluton's contact (Riklin, 1983).

Specimens of the Calcare di Angolo were collected in a section perpendicular to the pluton's contact starting at a distance of 4 km and ending at 65 m from the contact (Fig. 1b and c). The collected samples underwent peak metamorphic temperatures between 275 to more than 630 °C. In the last few tens of meters to the pluton, the sedimentary layering is rotated parallel to the vertical orientation of the contact, probably as a consequence of the pluton's emplacement. In order to avoid a deformational influence on grain growth, no samples at distances smaller than 65 m were collected. This sampling procedure followed an earlier strategy of Schmid (1997) and Herwegh and Berger (2003), who collected samples of the Calcare di Dosso dei Morti, which pass laterally into the Calcare di Angolo. The Calcare di Dosso dei Morti represent former stromatoporid reefs and are recrystallized by contact metamorphism as white, coarse-grained (up to several cm large calcite crystals), almost pure calcite marbles (Brack, 1983). The lithology of the Calcare di Angolo was chosen for this study due to the wide range in second-phase content. As a great advantage, the effect of variable second-phase contents on grain growth of calcite as dominant matrix phase can be tracked down.

3. Analytical methods

To identify the bulk mineralogy of the second phases, thin section analysis and XRD analytics were carried out. In the case of mineralogical layering, clearly visible by dark and lighter domains, we separated the individual layers mechanically and crushed and milled them into powder. In order to preserve the dolomite phase, separation of the calcite phase from sample powders was done using dilute (0.25%) hydrochloric acid. The residual material was cleaned with ethanol and air dried. The remaining powder of the insoluble residue, was then analyzed for mineral phases by means of X-ray diffraction (XRD) on a Panalytical X'Pert-Pro X-ray diffractometer. This instrument is equipped with a Cu-anode tube ($K\alpha_1$, $\lambda = 1.5406$ Å) set to operate at 40 kV and 40 mA and cover a 2-theta range from 4° to 40°.

For a detailed microstructural analysis the samples were treated in two different manners:

(i) All specimens were cut into thin sections oriented perpendicular to the sedimentary layering. To accentuate the grain and interface boundaries of calcite and second-phase particles, thin sections were first polished and then treated by two-step etching following the procedure described in Herwegh (2000). Prepared in this way, digital backscatter electron (BE-) images of the thin sections were used for grain boundary analyzes. In addition, energy dispersive X-ray spectrometry (EDX) was applied in order to identify the containing mineral phases in general and to visualize size and distribution of second phases by element (Ca, Si, Al, Mg, Na, K, Fe, Ti, P) mapping in particular. Electron microscopy was performed on a Cam Scan (CS4 with a Pioneer light element EDX detector) equipped with a Noran Voyager 4 image acquisition system and a Zeiss EVO 50 (with a Sapphire light element EDX detector) scanning electron microscope (SEM). For these analyzes, only specimen areas with homogeneous second-phase distributions were chosen, i.e., areas devoid of veins, calcite vugs and voids, fossil fragments, porphyroblasts and second-phase clusters. After the data acquisition by SEM, grain boundaries of all phases were traced manually and element maps were combined to be assigned to the different mineral phases using Adobe Photoshop. Size, distribution and volume fraction of second phases and calcite matrix were measured by using the image analysis software Image SXM (Barrett, 2008, www.liv.ac.uk/~sdb/ImageSXM) analogous to Herwegh (2000), Ebert et al. (2008) and Brodhag and Herwegh (2009). The resulting grain areas (for largest D_{cc}: 94 grains, smallest D_{cc}: 1447 grains) were used to determine the mean grain size for the calcite matrix (D_{cc}), which is given as area weighted value (for details see Ebert et al., 2007a). The volume fraction (f_p) and the mean grain size (d_p) for second phases like dolomite, white and dark mica, feldspars, tremolite, diopside, quartz, ores and apatite were calculated on the base of their grain areas and the calculation of the corresponding equivalent circular diameter.

(ii) In addition to the previous approach, electron backscatter diffraction (e.g., Adams et al., 1993; Prior et al., 1996) in combination with element mapping were performed on the Zeiss EVO 50 equipped with a DigiView II EBSD camera and the OIM data acquisition and image analysis software (AMETEK, TSL). These measurements were carried out under variable pressure conditions (10 Pa) at an acceleration voltage of 20 kV, a beam current of 10 nA and step sizes between 1.5 and 3 μm. Prior to these measurements, the samples were polished and lapped with colloidal silica (Syton) for about 2 h. Image analysis was followed along the steps described in (i). In order to exclude a potential effect of deformation on the microstructural evolution of the samples, the degree of crystallographic preferred orientation of calcite was checked on the base of stereographic projections and the texture index J (Bunge, 1982). Only samples with random c-axis distributions of calcite were used in the context of this study.

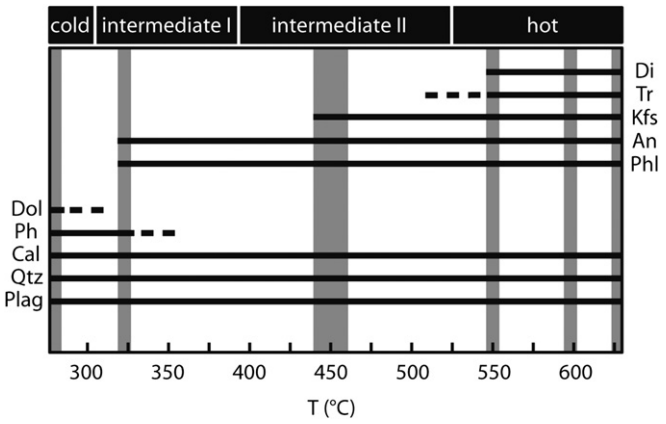

Fig. 2. Mineral assemblages for cold, intermediate I and II, and hot sample groups. Temperature ranges of the collected samples are marked in gray. Plag = Plagioclase, Qtz = Quartz, Cal = Calcite, Ph = Phengite, Dol = Dolomite, Phl = Phlogopite, An = Anorthite, Kfs = K-feldspar, Tr = Tremolite, Di = Diopside.

Temperature estimates of the sample locations were taken from the thermal model calculated by Herwegh and Berger (2003).

Table 1
Summary of the database of the microstructures analyzed in this study.

sample	Distance to pluton (m)	Temperature (°C)	D_{cc} (μm)	d_p (μm)	f_p	Z (μm)	No of cc grains	No of sp grains
SB05–07.1	65	630	61.04	19.98	0.285	70.11	789	1070
SB05–07.2	65	630	40.77	16.86	0.3751	44.95	489	539
SB05–07.4	65	630	113.27	19.10	0.12448	153.45	345	458
SB05–09.1	175	595	1079.93	77.63	0.1136	683.34	221	528
SB05–09.2	175	595	1001.75	66.10	0.1083	610.32	293	652
SB05-11.2a	315	550	2273.80	127.34	0.07888	1614.33	93	173
SB05-11.2b	315	550	4262.46	144.21	0.045595	3162.90	59	104
SB05–18.3	842	445	19.08	12.50	0.2253	55.50	1446	216
SB05–19.1	842	445	204.61	20.91	0.050778	411.76	391	331
SB05–19.2	842	445	164.67	17.19	0.05556	309.35	201	186
SB05–20.1	842	445	45.41	21.74	0.253	85.92	568	90
SB05–20.2	842	445	114.77	21.57	0.046267	466.17	883	137
SB05–21.1	783	455	391.38	53.28	0.002725	19552.07	429	14
SB05–21.2	783	455	676.33	101.19	0.003	33731.43	538	7
SB05–22.2	783	455	314.70	23.21	0.0004	58030.25	406	9
SB05–22.3	783	455	210.38	33.57	0.0012	27972.08	408	6
SB05–32.1	2190	325	77.53	21.59	0.1023	211.07	1096	109
SB05–32.2	2190	325	72.34	14.44	0.024712	584.53	413	37
SB05–33.1	2190	325	224.60	46.14	0.02206	2091.35	252	26
SB05–33.2	2190	325	234.86	52.75	0.1935	272.63	1561	201
SB05–34.1	2190	325	28.14	17.77	0.35786	49.65	297	307
SB05–34.1 b	2190	325	38.95	8.49	0.28533	29.77	180	112
SB05–34.2	2190	325	43.51	15.84	0.2859	55.39	397	401
SB05–34.2 b	2190	325	66.84	7.38	0.031561	233.70	613	452
SB05–34.3	2190	325	64.03	16.62	0.1309	126.96	811	301
SB05-42	>4000	275	15.76	7.61	0.4806	15.82	750	1123
SB05-44	>4000	275	9.67	11.28	0.496437	10.61	811	1525

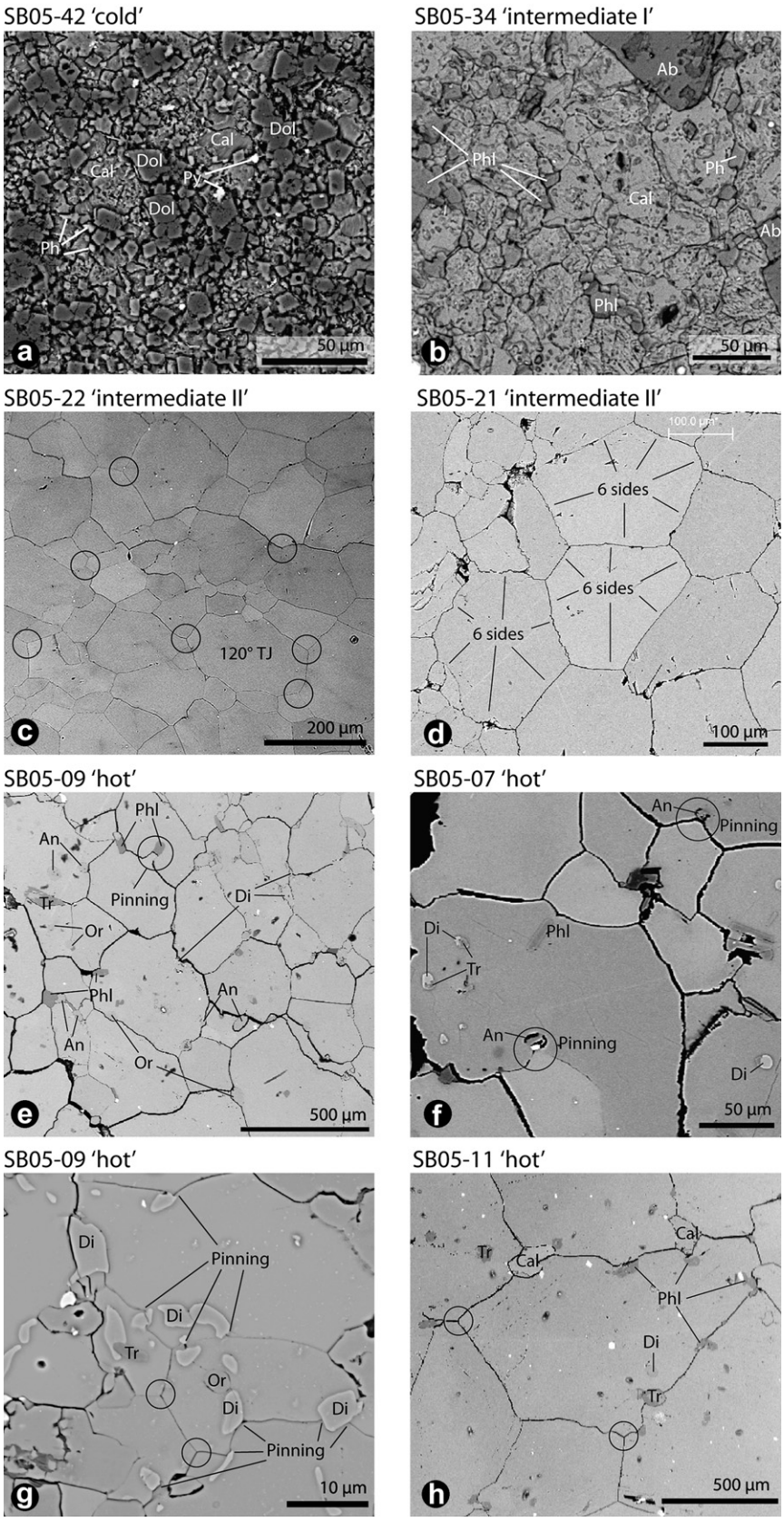

Fig. 3. SEM micrographs of typical microstructures. a) Microstructure of sample SB05-42 ('cold') shows very small calcite grain sizes but, in comparison to the calcite grains size D_{cc}, a relatively large second-phase grain size. Dolomites are hypidiomorphic to idiomorphic and are present in the sample with a very high second-phase volume fraction f_p. b) Sample SB05-34 ('intermediate I') has larger calcite grain sizes. Phlogopites are present for the first time in this sample group (see also Fig. 2). On the upper rim of the micrograph a part of an albite porphyroblast is visible. c) and d) 'Intermediate II' samples SB05-21 and −22 are relatively poor in second-phase volume fraction. Calcite grains show straight grain boundaries and comprise perfectly equilibrated 120° dihedral triple junctions (circles). Other evidence of equilibration is the formations of six-sided grains. e) Microstructure of

Modeling of the temperature distribution is based on a simple box-type 3D model. In the now expanded sampling area, the temperature distribution is somewhat more complicated owing to local deviation from a simple planar geometry of the vertical contact. In order to allow the use of the thermal model of Herwegh and Berger (2003) and Berger and Herwegh (2004), the sample locations were projected into a profile oriented perpendicularly to the pluton's contact by taking the locations and projecting them parallel to the contact into the profile section. For that reason, distance-to-pluton estimates are based on contour outlines at regular distances to the pluton contact as exposed at the surface. This approach is justified because of the vertical orientation of the Re di Castello pluton in the area investigated. The obtained distances then relate to the temperature estimates of Herwegh and Berger (2003). In order to gain information on the quality of the previously modeled temperatures, the second-phase mineral assemblages were compared to the mineral stability fields of petrogenetic grids showing a suitable correlation.

4. Results

4.1. Sample characterization

The suite of samples was collected in a contact metamorphic aureole with decreasing maximum temperatures from the contact to the unmetamorphosed starting material (Fig. 1; see above). We select different samples, but also investigate the microstructure of different layers within one sample. The Calcare di Angolo are characterized by intercalated calcite-rich layers and more marly layers, which is useful to show the difference in grain coarsening behavior with different volume fraction of second-phase particles. The matrix phase in all samples is calcite, while all other mineral phases are referred to as second phases and their individual grains as second-phase (sp) particles. For a general overview of mineral phases for each temperature group, see Fig. 2.

In general, the mean grain sizes (D_{cc}) of matrix calcite increase from the weakly metamorphosed material to the contact and are accompanied by a straightening of calcite grain boundaries and an increasing number of equilibrated triple junctions characterized by 120° dihedral angles. In light of the second phases located on calcite grain boundaries and included in calcite grains, for both the mean grain sizes (d_p) increase, but the sizes of the included second phases are smaller than the corresponding ones at the grain boundaries. Additionally, the number of second phases included in the calcite grains rises with increasing temperature. Detailed quantitative information of each sample can be derived from Table 1.

The emplacement of a pluton is associated with deformation within the pluton itself but also at it rims, as also visible by the steeply oriented bedding of the contact metamorphic sediments within the first 65 m (see above). Although we cannot completely exclude the presence of a small deviatoric stress component during contact metamorphism for the samples at larger distances to the pluton's contact, the absence of typical deformation microstructures like crystallographic preferred orientations (CPO), grain shape preferred orientations (SPO), pervasive foliations or dynamic recrystallization microstructures indicate that a potential deviatoric stress component must have been much smaller in comparison to those found in shear zones. For that reason we can consider the situation in the area investigated to be rather close to true static conditions.

The weakly metamorphosed materials (*SB05-42, SB05-44,* Fig. 3a) referred to in the following as 'cold' samples represent typical diagenetic limestones, which are hardly affected by the intrusion. Fossils, like crinoid columnals or reef debris deriving from the Calcare di Dosso dei Morti reef sediments can locally still be found embedded in a micritic matrix. In addition, typical diagenetic features like sparitic vugs and voids still exist in these dark gray limestones. The mean grain size of the calcite matrix is small (15.8 and 9.7 μm) and the second-phase grain size d_p is half of D_{cc}. The grain size distribution is slightly right-skewed and covers grain size intervals between 2 and 20 μm (Fig. 4). In the two samples investigated (Table 1), the volume fraction (f_p) of the second phases ($f_p \sim 0.5$) is only slightly lower than that of the matrix calcite. The dominant second phases are dolomite and white mica (illite). Dolomite grains in both samples have idiomorphic to hypidiomorphic lozenge shapes (Fig. 3a). Note that dolomite is preserved in these two samples only. Furthermore, plagioclase, quartz, and accessory titanite and pyrite are present. Due to the very high volume fraction of second phases, calcite grain boundaries mostly comprise a contact to second phases and calcite triple junctions are rare. Particularly, dolomite forms a large number of sp–calcite interfaces. In contrast to samples derived from higher metamorphic grades, no second-phase grains are included in calcite grains at these low temperature conditions.

A first set of metamorphic samples (*SB05-32, SB05-33, SB05-34,* Fig. 3b) was collected at an outcrop about 2200 m away from the intrusion contact. These samples underwent peak metamorphic temperatures of around 325 °C and are called in the following 'intermediate I' samples. D_{cc} values (66–234 μm) are higher for samples with relatively low second-phase content than for the 'cold' ones described above, but can be as small as 28 μm for samples with high second-phase volume fraction. The asymmetric shape of the grain size distribution persists but the smallest and largest grain size intervals of calcite shift toward larger values of 15 μm and 120 μm, respectively (Fig. 4). Additionally the frequency of the smallest grain size class increases. Analogous to the scatter in D_{cc}, the grain sizes of second phases also show a wide spread ranging from 7.4 to 52.8 μm. Very few second-phase grains (on average less than $f_p = 0.012$), but of all mineral phases present, are included in matrix grains. Calcite grain boundaries are less often occupied by second phases owing to the smaller volume fraction than in the 'cold' samples. Therefore, pure calcite grain boundary triple junctions are more frequent, but only few of them show equilibrated 120° dihedral angles. The second phases are phengite, plagioclase and quartz. Some plagioclase grains are of idiomorphic shape typical for porphyroblastic growth and show decompositional alterations (Fig. 3b). The first phlogopite appears (*SB05-34*, Fig. 3b) with mainly xenomorphic shapes, but some individuals are hypidiomorphic to idiomorphic. Xenomorphic, small and very scarce grains of anorthite and orthoclase are present in some sections of the samples.

A second set of metamorphic samples (*SB05-18 to SB05-22*, Fig. 3c and d) was collected at two different outcrops about 780 and 840 m away from the contact, affected by peak metamorphic temperatures of 445–455 °C. For these 'intermediate II' specimens, D_{cc} and d_p vary not only from sample to sample, but also in different sections of the samples (D_{cc}: 19–676 μm; d_p: 12.5–101.2 μm). In terms of grain size distributions of the matrix grains, a further increase in both the grain size range and the minimum and maximum grain size intervals occur, while the shape of the grain size distribution still is right-skewed (Fig. 4). Almost all second-phase grains are located along matrix

a 'hot' sample (SB05-09): Calcite grain boundaries can be straight but also curved at locations where pinning of the calcite grain boundaries by second phases occurs. Tremolite and diopside are newly formed mineral phases in this sample group. f) Micrograph of SB05-07 ('hot') shows pinning of calcite grain boundaries by individual second-phase particles. g) and h) calcite grain boundaries are pinned by multiple second-phase particles and by 120° triple junctions (circles). Note the differences in scale between the different micrographs.

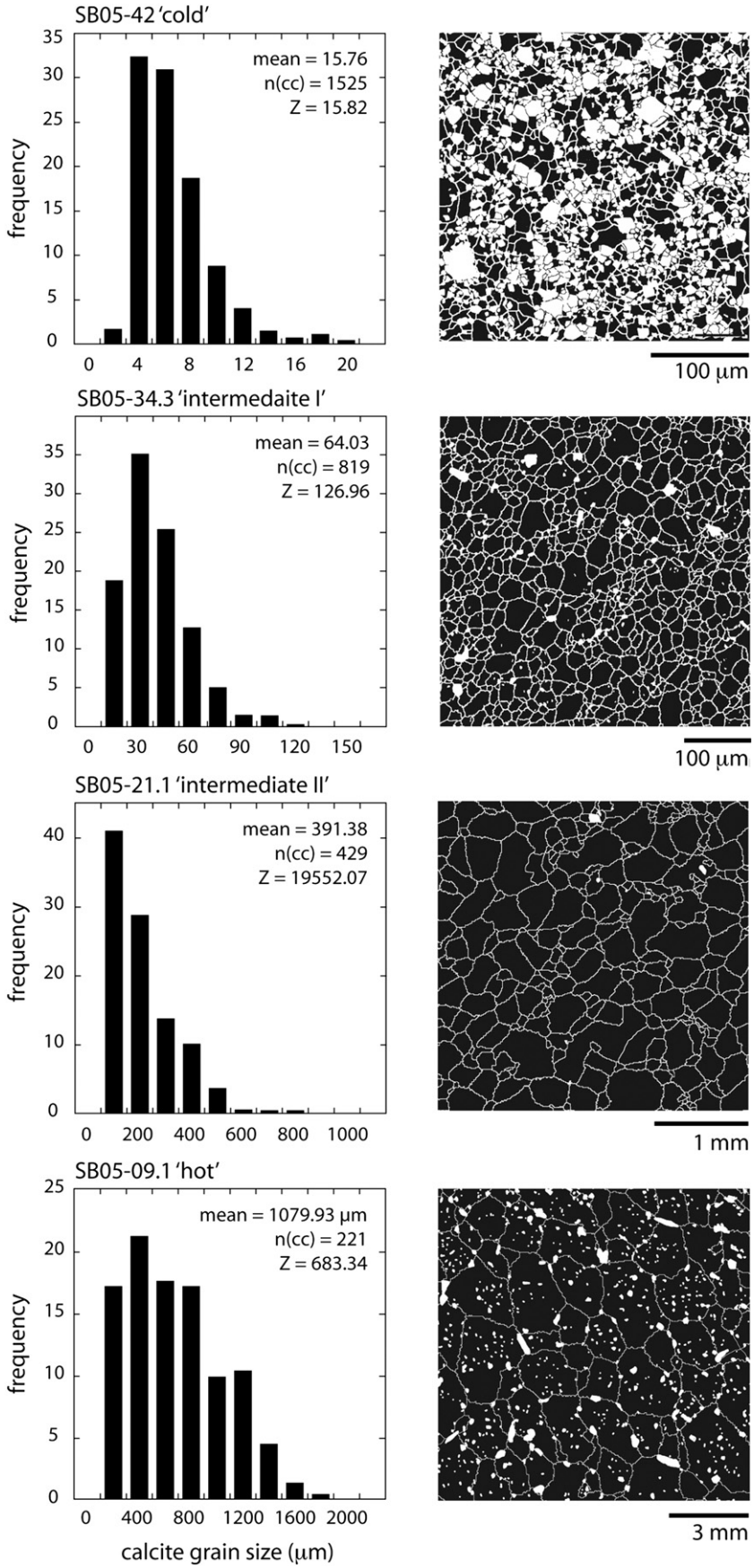
SB05-42 'cold'
mean = 15.76
n(cc) = 1525
Z = 15.82
frequency
100 µm
SB05-34.3 'intermedaite I'
mean = 64.03
n(cc) = 819
Z = 126.96
frequency
100 µm
SB05-21.1 'intermediate II'
mean = 391.38
n(cc) = 429
Z = 19552.07
frequency
1 mm
SB05-09.1 'hot'
mean = 1079.93 µm
n(cc) = 221
Z = 683.34
frequency
3 mm
calcite grain size (µm)

grain boundaries and inclusions of second phases in calcite are very rare, but they exist for each mineral phase. Calcite grain boundaries of the samples with larger grain sizes and smaller f_p are straight and comprise perfectly equilibrated 120° dihedral triple junctions (Fig. 3c and d). As a consequence, the entire aggregates show equi-granular foam-type microstructures. The volume fractions of second phases generally are quite low in this group and most samples are relatively poor in mica. In contrast to the 'intermediate I' group, phengite is not present in any of the samples. Further phases are quartz, K-feldspar, plagioclase and titanite, but all are very rare to accessory. Exceptions are saussuritizated plagioclase porphyroblasts with atoll texture (*SB05-18*), and perfectly idiomorphic anorthites, lozenge to wedge shaped titanites and round quartz grains (*SB05-20*). Sample *SB05-21* is completely devoid of any silica bearing mineral phase.

With distances from 315 to 65 m, the 'hot' samples *(SB05-07, SB05-09, SB05-11*, Fig. 3e–h) are situated closest to the pluton's contact suggesting peak metamorphic temperatures in the range of 550 °C–630 °C. The range of D_{cc}-values for this group is largest. The biggest D_{cc} value of 4262.5 μm is two orders of magnitude larger than the smallest one (40.8 μm). The calcite grain size distributions remain right-skewed but the grain size range further broadens showing larger spreads than the samples subjected to lower temperatures (Fig. 4). Second mineral phases are not only located on grain boundaries, but compared to the less metamorphosed samples, a relatively high amount of second phases is also included in the interior of calcite grains (f_p up to 0.056, see Fig. 3e–h and Fig. 4). The grain sizes for second phases located at grain boundaries (max. d_p = 182.6 μm), as well as for included ones (max. d_p = 118.8 μm, *SB05-11.2b*), are both larger than those of the less metamorphosed samples. Again, every mineral is found as inclusions in calcite, which is also the case for the newly formed phases tremolite and diopside. To some extent, matrix grain boundaries comprising second phases show clear pinning characteristics in form of grain boundary segments that are highly curved and lobate in the close vicinity of second phases (see circles in Fig. 3e and f). Calcite grain boundaries that are not in contact with second phases, are in general very straight and converge into triple junctions with 120° dihedral angles (Fig. 3g and h). Generally, the matrix microstructure in all three samples is very equi-granular. Tremolite grain shapes are hypidiomorphic elongated and in some parts of the samples, they occur as porphyroblasts. Phlogopite, K-feldspar and plagioclase are present, as well as accessories like quartz, titanite, pyrite and apatite.

4.2. Quantitative microstructures

In addition to the above given average sizes of the calcite and second-phase grains, we need a quantitative description of the relationship between the second phases and the matrix. For this purpose, we will focus in the following on two major data sets: (1) nearest neighbor relations between both calcite–calcite and sp–sp grains and (2) relations between matrix grain size, second-phase grain size and their volume fraction, i.e., a relationship which is referred to in literature as Zener relation (e.g., see review of Manohar et al., 1998).

4.3. Nearest neighbor relationships

Based on the geometric centers of the calcite and second phases quantified in the microfabrics by the aforementioned image analysis approach, the distances of the five nearest calcite and second phase neighbors on calcite grain boundaries, were calculated for each calcite and second-phase grain, respectively, using a nearest neighbor calculation (NNC, written by Mark Jessell). Visualized in form of distance to frequency histograms, the distribution of the mean distances of calcite and second phases can be detected and correlated with each other (Fig. 5). In this context, we introduce a correlation parameter (K), which is defined by

$$K = M_{cc}/M_{sp} \quad (2)$$

where M_{cc} and M_{sp} represent the modes of the nearest neighbor distributions of the calcite and second-phase grains, respectively. K values larger than 1 signify closer average spacing of second phases than the spacing, i.e., the grain diameter, of the calcite grains and vice versa.

The analyzed samples can be divided into three groups depending on the relation of the spacing between the matrix grains to the spacing between the second phases. For the first group, distances between second phases are smaller than distances between the matrix grain cores yielding in a correlation parameter larger than 1 (*SB05-09.1* and *-42*, Fig. 5 top and Table 1). Note that samples of each temperature ('cold' to 'hot') are found in group I covering a large range in second-phase volume fractions from 0.49 to 0.046. The second group shows just the opposite relation between spacing of matrix and second-phase grains, resulting in a correlation parameter smaller than 1 (*SB05-21.1*, Fig. 5). Again, samples of almost

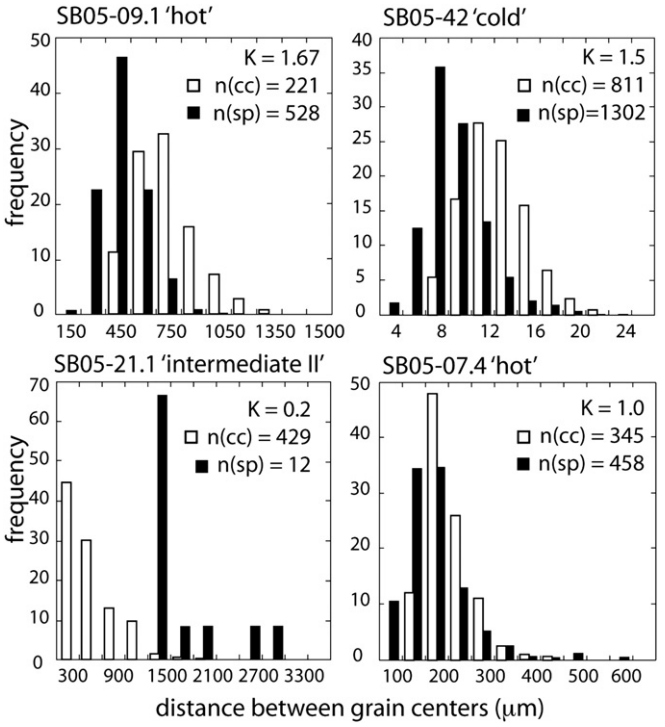

Fig. 5. Nearest neighbor distributions for calcite–calcite (white) and sp–sp (black) grains. On base of the correlation parameter K, i.e., the spacing of calcites (cc) divided by the spacing of second phase (sp) particles, samples can be organized into three groups, independent of temperature. Samples with $K > 1$ have a smaller spacing between second-phase particles compared to that between calcite grains, while samples with a larger spacing of sp particles show $K < 1$. If spacing of cc–cc and sp–sp grains are both equal, $K = 1$.

Fig. 4. Characteristic crystal size distributions (CSD) for the four different temperature groups. Right column shows grain boundary maps. Calcite grains are black, calcite grain boundaries and second-phase particles are white. Left column displays frequency of area weighted mean grain sizes as well as the number of analyzed calcite grains n(cc) and the Zener value Z. Crystal size distribution (CSD) shift from 'cold' to 'hot' sample groups to larger calcite grain sizes. While all samples show right-skewed distributions, the peak of SB05-09 is broader in comparison to the other samples.

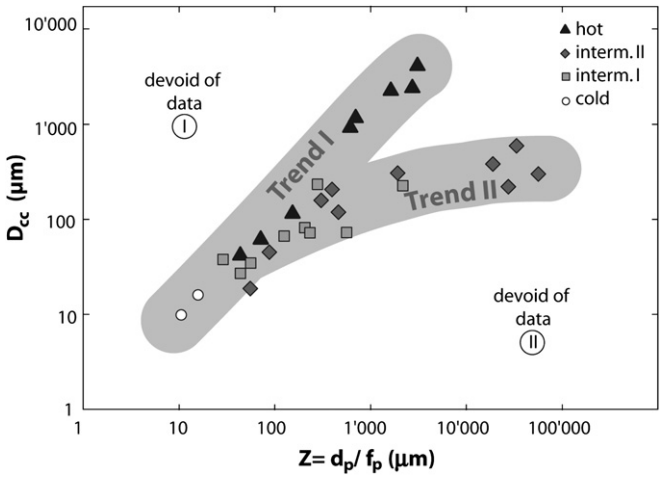

Fig. 6. Calcite matrix mean grain size in relation to the Zener parameter. Plot of calcite grain size D_{cc} versus the Zener parameter Z: In general, calcite grain size D_{cc} is larger with increasing temperature and Zener value Z. Two trends are clearly visible in the Zener diagram: a steep trend (I) with sample data from 'cold' to 'hot' and a curved trend (II) with mainly sample data of 'intermediate I' and 'II'. Note that on the left side above trend I (high D_{cc} but low Z) and the right side below trend II (small D_{cc} but high Z) there are two fields devoid of any data. Symbols for the different temperature groups are given in the legend.

every temperature are present in this group, and the f_p range is large as well but shifted toward smaller values (0.22–0.0004) compared to group I. Samples with exactly the same spacing values for second-phase particles and calcites, i.e., $K = 1$ (cf. Fig. 8), form the third group. Samples *SB05-07.4*, *-32.2* and *-34.2* belong to this group (see Table 1). Similar to the widening of the range of grain size distributions, the nearest neighbor spacing between individual second-phase particles and the nearest neighbor spacing between calcite grains increase with increasing temperature as well as with increasing Z for samples with identical temperature.

4.4. The link between second-phase particle sizes, their fractions and the matrix grain size (Zener diagram)

While the crystal size distribution (CSD) and the nearest neighbor relation take only the size and dispersion of second phases into account, the Zener diagram (e.g., Berger and Herwegh, 2004; Herwegh et al., 2005; Ebert et al., 2007a,b; Brodhag and Herwegh, 2009) represents an appropriate way to unravel the influence of second phases on the grain size of the matrix phase. The Zener diagram links the matrix grain size D_{cc} with the Zener parameter, i.e., with the ratio between grain size (d_p) and volume fraction (f_p) of second phases. In Fig. 6, each data point represents the mean values of an analyzed microstructural area, generally consisting of several hundreds of calcite grains. The two most impure samples (*SB05-42* and *-44*) with smallest Z and highest volume fraction are situated in the lower left corner of the graph, while with increasing purity, i.e., higher Z, data points shift toward the right side in the Zener diagram (Fig. 6). In respect of temperature, samples with higher peak metamorphic temperatures have generally a larger D_{cc} than colder samples but same Z value. But note as well that some samples with the same temperature and similar Z can have a different D_{cc}, as it is the case for samples *SB05-19.1* and *-20.2*, and *SB05-34.1* and *-34.2* (see Table 1). Vice versa, samples of the same temperature group can have a similar D_{cc} but different Z values (see *SB05-19.1* and *-22.3*, and *SB05-33.1* and *-33.2*, Table 1).

Despite these apparent inconsistencies, two general trends can be constituted for the Zener diagrams of our Adamello samples: Trend I is characterized by a distinct straight and steep incline, where D_{cc} increases intensely with relatively small changes in Z. Trend II is rather diffuse but is defined by a weaker increase in D_{cc} over a large range of Z values. While the slope of the trend is somewhat steeper at low Z values and flatter for higher ones, trend II appears slightly curved in the Zener diagram despite the logarithmic scale of the axes. Due to the large scatter of data points at medium Z values of around 200 to 500 and D_{cc} between 65 and 240 µm, the area where trend II branches off the steeper trend I is not clearly visible in this type of diagram. Note that individual samples from both groups, 'intermediate I' and 'intermediate II' temperatures can be found on both trends, while all the 'hot' and the two investigated 'cold' samples are situated on trend I exclusively.

Interestingly, there are two fields in our diagram that are completely devoid of any data point. In the upper left quadrant, i.e., above trend I, there exist no calcite grain sizes for relatively small Z (i.e., small d_p in combination with high f_p, field I). Also, very pure samples with large Z but small D_{cc}, which would plot in the lower right corner, do not exist in our suite of samples (field II). These two fields of missing data points are quite important as will be discussed below.

5. Discussion

Second-phase minerals can have dramatic effects on the microstructure of polymineralic rocks with a volumetrically dominating matrix phase, because they can either induce a retardation of the velocity of migrating grain boundaries via temporally restricted pinning or they can immobilize a grain boundary due to a complete pinning. The physical reason for these two behaviors is related to dragging forces imposed by the second phases on the moving grain boundaries of the matrix phase, which counteracts surface energy as major driving force of grain growth (e.g., see Evans et al., 2001 and references therein).

In light of the samples investigated in this study, the Zener diagram (Fig. 6) demonstrates that the grain sizes of the matrix calcite in all samples are affected by second phases allowing a discrimination of the two trends I and II mentioned above. But what exactly is the microphysical influence of the second phases and why do samples with same temperature-time history and similar Z result in different matrix grain sizes as manifest by the two trends in Fig. 6. All these data represent the ambient microstructural relation between matrix grain size and sp minerals, which, however, evolved over a T–t history. The problem is even more complex because no unique T–t path exists but it rather changes for the different sample locations, owing to their varying distances to the pluton's contact. For that reason, we generalized potential T–t effects by grouping locations with similar ranges of distances to the pluton into the aforementioned groups 'hot', 'intermediate I and II' and 'cold'. In the context of the temperature dependent influence of the second phases on the calcite grain boundary, the following points need to be addressed for each of these groups:

- Which regime of pinning can be detected in the samples?
- Do the pinning processes change with time/temperature?
- What is the effect of the pinning on the final matrix grain size?

In light of these questions, the Zener diagram with its restriction to the mean values of matrix and second-phase grain size as well as to the volume fraction of the latter will give no unique answer. We therefore have to combine on one hand the information about dispersion of second phases as obtained by the nearest neighbor calculation and the Zener diagram. On the other hand, we have to scrutinize the specific contribution of the size and volume fraction

of the second phases to the microstructural evolution of the aggregates.

Associated with the metamorphic evolution of the samples, the changes in the stability fields of some of the second-phase minerals induce mineral reactions (see Fig. 2). The mineral reactions in this KCMASHC-system have been investigated (e.g., Bucher and Frey, 1994; Cui et al., 2003; Nabelek, 2007). In terms of the evolution of the modal composition of our rock samples as a function of changing metamorphic conditions, two general sequences have to be discriminated: (1) The total consumption of diagenetic dolomite due to the formation of Mg-bearing metamorphic phases during an early stage of metamorphism (e.g., formation of Mg-phengite, Mg solid solution in calcite) and (2) the transformation of existing metamorphic phases enclosed with a further increase of metamorphic conditions. Most relevant reactions are net transfer reactions including the nucleation of new phases. The sites of nucleation of these new phases may be restricted to locations of pre-existing second phases for elevated temperature reactions (e.g., tremolite + calcite + quartz = diopside + CO_2 + H_2O). In this case, the physical pinning of a calcite grain boundary by a pre-existing second phase will be preserved during the reaction but might be modified due to changes in grain size and shape of the new reaction products. Despite the latter limitation, nucleation at pre-existing sites of second phases allows treatment of the polymineralic aggregates as a two-phase system consisting of calcite and second phases only. This simplification of the complex system is justified, because we will restrict in the following discussion to the general physical interactions between existing second phases and the calcite grain boundaries only, independent of the mineralogy of the second phase. Potential effects related to differences in grain shapes are neglected for the moment but are extensively discussed in Berger et al. (2010).

More problematic in light of the suggested simplification is the major change from dolomite-calcite bearing carbonates toward calcitic carbonates. All reactions consuming the dolomite will change the microstructure because of (i) a significant loss of CO_2 and (ii) a volume change during reactions since all these reactions include a fluid component. Hence, major changes in the volume fractions of matrix and second phases will occur during the early stages of metamorphism (below intermediate I conditions). Therefore, this stage of transformation cannot be included in the following geometric considerations. However, several minerals like phlogopite are stable for a long time and over a considerable range of metamorphic temperatures of the microstructural evolution allowing the exploration of their physical interactions with the matrix phase. We approximate this goal by looking on the geometrical evolution in a first step, but we are well aware, that this approach represents a simplification (for more details see Berger et al., 2010).

Due to the complexity of the entire system, we will treat first the pinning of matrix grain boundaries by second phases at constant temperature and will then focus on coupled grain coarsening of the aggregate as a function of variable temperatures.

5.1. Evidences for pinning of matrix grain boundaries

In a microstructural point of view, pinning is most evident by the changes in calcite grain size as a function of the varying second-phase volume fractions (Fig. 7), which is independent of the local mineralogy. The same two trends (I and II) as in the Zener diagram of Fig. 6 are visible in this D_{cc}–f_p relation, and samples with the identical f_p developed different calcite grain sizes.

On the grain scale, an indication that sp particles can pin grain boundaries is demonstrated in the SEM image of Fig. 3e, where a calcite grain boundary of sample *SB05-09* is highly curved due to

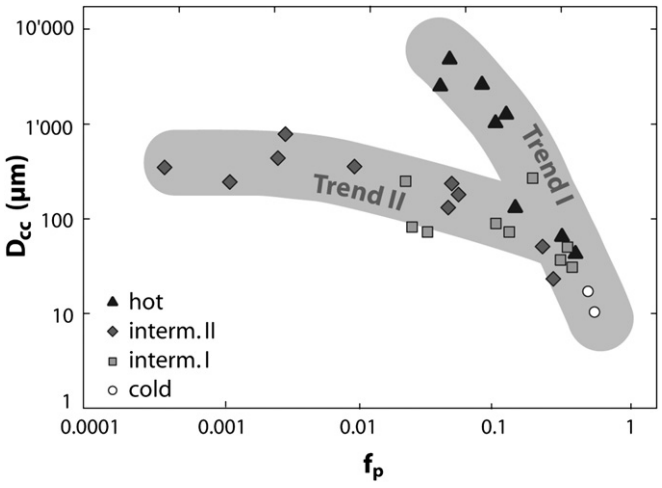

Fig. 7. Calcite matrix grain size in relation to the volume fraction f_p. Like in the Zener diagram of Fig. 6, two trends are visible. Calcite grain sizes change as a function of second-phase volume fraction f_p and the temperature *T*. Samples with high f_p of second phases have small calcite grain sizes, while hotter samples evolved larger grain size compared to colder samples with similar f_p.

the pinning by a phlogopite grain. However, situations as presented in Fig. 3e–h express a transitional stage between a pinned grain boundary and a grain boundary completely detached from the second phase. Such geometric relations reflect frozen natural examples of dynamic situations, where the high curvature of the grain boundaries at the moment of detachment from the second phases forces the grain boundary to adjust at high velocity to the more favored straight to slightly curved geometries (see the same effect in analog experiments of Brodhag and Herwegh, 2009; their Fig. 6). As a consequence, the preservation of matrix grain boundaries which are still attached to a second phase but show a high curvature at the stage just before detaching (like the situation in Fig. 3e) is quite rare.

5.2. Differences in grain boundary pinning at constant temperatures

The variations in calcite grain size at similar temperatures must require an explanation. The data presented above indicate that the grain size variation can primarily be related to amount, size and distribution of second-phase particles. In order to understand the processes behind these relationships, we will briefly summarize the meaning of both the Zener relationship (e.g., see Evans et al., 2001) and the nearest neighbor relationships.

Combining the nearest neighbor data with the Zener diagram (Fig. 8) results in a perfect match between the three groups (NNC) and the two trends (Zener diagram). Samples with a correlation parameter $K > 1$ are situated on trend I of the Zener diagram, while samples with $K < 1$ are either located on trend II or at the transition where trend II branches of from I. Samples with $K = 1$ are located in the area of branching off and, therefore, cannot be assigned clearly to any of the two trends. The geometrical link between the correlation parameter *K* and the Zener diagram can be visualized by a honeycomb microstructure of the matrix phase (Fig. 8). $K = 1$ represents an ideal case of a fully pinned matrix phase with honeycomb microstructure, where a second phase is located at every second triple junction. In this way, three triple junctions and therefore all six grain boundary segments of a matrix grain are affected by a second phase and the spacing between grain centers among matrix grains and grain centers among second phases is identical. Thus, a matrix grain is in contact with three second-phase

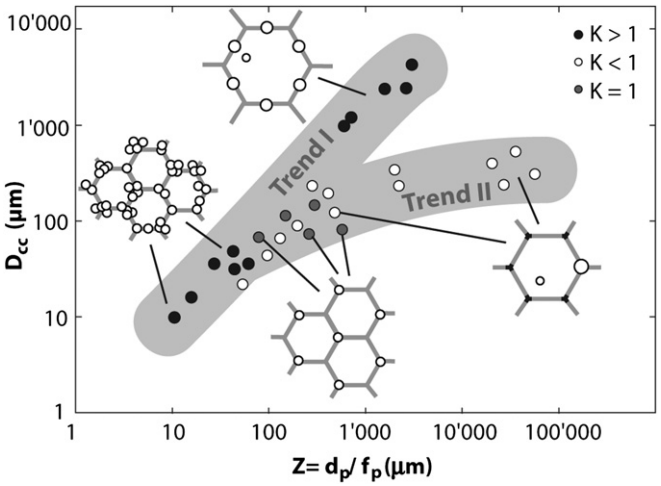

Fig. 8. The link between Zener diagram, K value and microstructure Graph of Fig. 6 with generalized microstructures and K values: The three different groups of K values resulting from nearest neighbor relationships and the two trends of the Zener diagram show a striking correlation. Samples with a correlation parameter $K > 1$ lie on trend I (black), while samples with $K < 1$ are situated on trend II (white). Samples with $K = 1$ (dark gray) belong to the scatter zone where trend II branches off from trend I. Schematic microstructures of the different situations (gray: matrix grain boundaries, white circles: second phases, black triple junctions).

particles, but shares them with its neighbor. In this sense, the K-factor is in relation with the Zener parameter Z, since Z is related to the average interparticle distance between the second phases. Several authors (e.g., Gladman, 1966; Hellman and Hillert, 1975; Evans et al., 2001) modified Zener's original equation:

$$D_{\max} = c^m \cdot \left(d_p / f_p^m\right) \tag{3}$$

where c is a constant and $D_{\max}$ the maximum matrix grain size and m is a geometric parameter that assigns the spatial location of the second phases in the aggregate. For the ideal case, where the second phases occupy triple junctions and are shared by three grains, m equals to 1/3 (Fig. 9). Second phases located on triple junctions represent a rather efficient regime of pinning that hardly can be overcome by the driving forces of a migrating grain boundary. In contrast, sp particles on grain boundary segments located between two triple junctions are shared by two neighbor grains ($m = 1/2$) and pin a migrating grain boundary less effectively compared to those located on triple junctions. To fully pin all six boundary segments of a matrix grain by this pinning regime, six second phases, which are shared by six neighbor grains, are required. Even more effective pinning occurs in the case where the second phases sit on triple junctions as well as on the grain boundaries between them, resulting in $m = 1/2 - 1/3 = 1/6$ (Fig. 9). Hence, the smaller m the more intense is the pinning of the boundaries of a matrix grain size. If m approaches zero, c^m and f_p^m are 1 and equation (3) reduces to

$$D_{\max} \Rightarrow d_p \tag{4}$$

where $D_{\max}$ depends only on d_p. Geometrically, this situation implies matrix grains that are completely surrounded by sp particles and the remaining space for an individual matrix grain is equal to d_p. On the contrary, when m approaches 1, c^m and f_p^m reduce to c and f_p, respectively resulting in

$$D_{\max} \Rightarrow c \cdot \left(d_p / f_p\right) \tag{5}$$

In this case, $D_{\max}$ depends mainly on f_p. As stated by Evans et al. (2001 and references therein) this case applies for relatively small d_p and a microstructure where many second-phase particles are included in the interior of the matrix grains.

Note that all these considerations are limited because they (i) are of purely geometric two-dimensional nature, (ii) are only valid for grain growth of a matrix phase with a non-growing second phase, (iii) are only valid for aggregates that undergo grain growth at constant temperature and (iv) do not incorporate additional parameters that affect the mobility of a grain boundary such as induced by the crystallographic misorientation of matrix neighbors at grain triple junctions (triple junction pinning, TJP; see Piazolo et al., 2005, 2006; Shvindlerman and Gottstein, 2005).

Looking at the samples investigated, relations with $K > 1$ imply a statistical distribution of more than three shared second-phase particles along a grain's surface in the case of a two-dimensional section, and $K < 1$ means that less than three particles are sitting on the grain's surface. In the latter case, m would be >1/2 because not enough second phases would be available to fully pin all boundary segments of a matrix grain. This latter pinning regime is called single particle pinning (SPP, Brodhag and Herwegh, 2009). Hence, to obtain completely immobile grain boundaries of the matrix phase for $K > 1$, triple junction pinning is required to occur in addition to single particle pinning. With respect to pinning of matrix grain boundaries, $K > 1$ reflects grain boundaries affected by multiple second-phase particles. Only in the case where second phases are located at least on every second triple junction (in the case of honeycomb structure three second-phase particles are required) a complete pinning is possible ($m = 1/3$). Otherwise a larger number of sp would be required for a complete

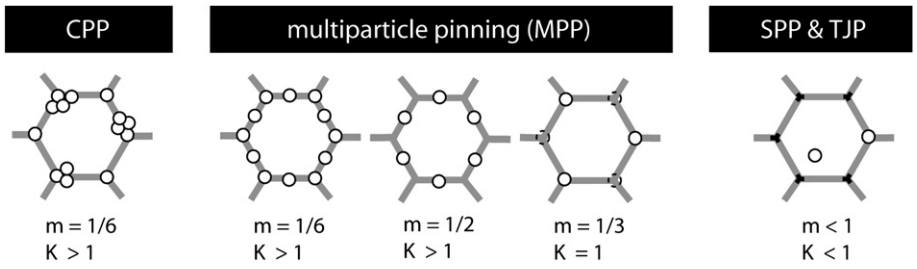

Fig. 9. Pinning types and related geometric factor m In the ideal case of a matrix with honeycomb microstructure, grains are fully pinned if the geometric parameter $m = 1/3$ (triple junctions) or 1/2 (grain boundary) depending on the spatial distribution of the sp particles. Second phases located on grain triple junctions pin more effective then sp grains situated on calcite grain boundaries, and therefore, less sp particles are required to pin a grain's boundaries completely. For low second-phase volume fractions f_p, m can approach 1 if most of the sp particles are included. In this case only single particle pinning (SPP) and triple junction pinning (TJP) will stabilize the grain size. Very small m signifies that the grain boundary is pinned by multiple particles (MPP) and/or clustered particles (CPP), which then are the dominating pinning types. K values are related to the spacing between calcite grains and second-phase particles, and are explained in the text.

immobilization of all boundaries of a grain (see above). These regimes of pinning are referred to as multiple particle (MPP) or clustered particle pinning (CPP) by Brodhag and Herwegh (2009).

Hitherto, pinning by more than one rigid particle along one matrix grain boundary is well described (e.g., Miodownik, 2005) and it is experimentally shown by Brodhag and Herwegh (2009) that pinning by multiple particles (MMP) has a stronger effect on the retardation of a migrating matrix grain boundary than pinning by single particles. Also, the pinning effect of larger sp particles is more enhanced compared to smaller ones as calculated by Manohar (1998) and in the case of large-sized clusters of second phases (clustered particle pinning, CPP) by Brodhag and Herwegh (2009).

Transferred to our samples, calcite grains of trend I ($K > 1$) are, therefore, in contact and influenced by several second-phase particles, i.e., affected by multiple particle pinning (see Fig. 3e and h) or clustered particle pinning (see Fig. 3a and g). Surface energy of the matrix grains is insufficient in these cases to overcome the pinning forces induced by several sp particles. Single particle pinning is the dominant regime for trend II microstructures (see Fig. 3f). In contrast to multiple particle pinning and clustered particle pinning, the matrix grain boundaries can be pinned temporarily in this case, allowing the detachment of the grain boundary from a sp particle at the moment the locally increased grain curvature overcomes the dragging force (see previous section). In addition to single particle pinning, equilibrated triple junctions (see Fig. 3c) can also contribute as pinning factor (triple junction pinning (TJP); Piazolo et al., 2005, 2006; Shvindlerman and Gottstein, 2005; Gottstein et al., 2006). Hence, with increasing grain size and the associated reduction in surface energy, single particle pinning in combination with triple junction pinning may also result in a complete immobilization as suggested by the rock analog experiments of Brodhag and Herwegh (2009).

5.3. Comparison with experiments

The aforementioned considerations on the relations between different grain sizes and their volume fraction assume stabilized grain sizes. In the case of regional metamorphic rocks with long exposure of the samples to elevated temperatures the measured grain size can be assumed to be more or less stabilized, because of the exponential grain growth behavior with time (Herwegh et al., 2005). In the case of long term isothermal conditions, as is the case for regional metamorphism, this means that the coarsening of the polymineralic aggregates continuous owing to the exponential form of the growth equation. Despite this continuation, however, the grain size increases per given time increment become so small that almost no grain size changes can be detected anymore leading to an apparent stabilization of the grain sizes after coarsening periods of millions of years. The situation differs in the case of contact metamorphic rocks, where such grain size stabilization is questionable, because the time of metamorphism is short. During contact metamorphism (i) fast grain coarsening per time increment exists over relatively short time periods only (thousands to ten thousands of years at elevated temperature) and (ii) an early freezing in of the metamorphic microstructures occurs because of the temperature drops, as early as a few ten thousands to one to two hundred thousand years after onset of the temperature rise (see Fig. 6 in Herwegh and Berger, 2003).

Recent rock analog experiments on grain coarsening in two-phase aggregates (norcamphor and non-gowing microbeads as second phases; see Bordhag and Herwegh, 2010) can be used to gain insights on the possible microstructural evolution of the Adamello samples (Fig. 10, see also Brodhag and Herwegh, 2009). The starting aggregates show small initial matrix grain sizes and interparticle distances of the second phases larger than the average

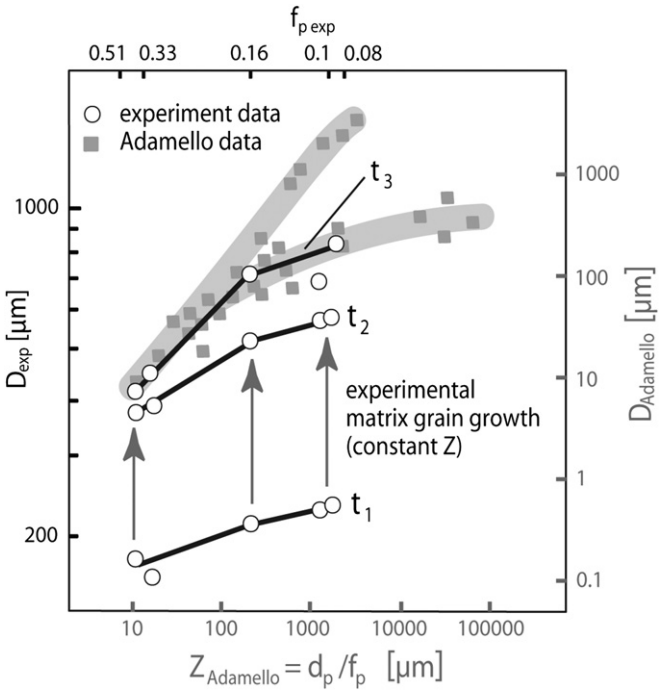

Fig. 10. Comparison of experimental studies and nature. Experimental rock analog studies by Brodhag and Herwegh performed on mixtures of polycrystalline norcamphor and glass beads (Fig. 9 modified, 2009) show a stabilized grain size (D_{exp}) trend for the norcamphor matrix (t_3, white circles, black axes labeling), which is similar to the analyzed Adamello samples (gray squares, gray axes labeling) on trend II (Fig. 6). For both, pinning types multiple particle pinning MPP and clustered particle pinning CPP are effective for high f_p of natural samples and experiments, respectively, while SPP and TJP influence low f_p matrices. The time steps t_1 and t_2 are the transient evolution stages of norcamphor matrix grains and could be used as an analog for the transient evolution stage of the Adamello samples, which is not preserved anymore owing to progressive grain coarsening. Arrows indicate the growth path of experimental matrix grains influenced by rigid non-growing sp particles.

matrix grain size. With the onset of coarsening, the latter will therefore be affected first by single particle pinning yielding in a straight trend line (see t_1, Fig. 10). With time and increasing matrix grain size, more and more second phases will influence individual matrix grains leading to a transition to multiparticle or even clustered particle pinning. Consequently, the matrix grains are pinned more severely at low compared to high Z values resulting in the curved slope at t_2 (Fig. 10). At some point, too many second phases affect the matrix grain boundaries such that any further increase in matrix grain size is impossible and the microstructure stabilizes in the aforementioned way. The resulting trend line t_3 of the experiments correlates in an excellent manner with the intermediate temperature trends of the Adamello samples (Fig. 10) implying that for latter similar stabilization might have occurred.

5.4. Calcite coarsening processes and their physical interactions with second-phase particles

The different pinning regimes and the change in their net contribution to the pinning of the matrix grains of the bulk aggregates were discussed as a function of time, regardless of the changes of second-phase particle sizes with time. Changes in sp grain sizes must have occurred in the Adamello samples where d_p increases proportionally to the increasing calcite grain size D_{cc} (Fig. 11). The simultaneous growth of second phases and matrix grains is referred to as coupled grain coarsening (Alexander et al., 1994). This observation is in agreement with studies of

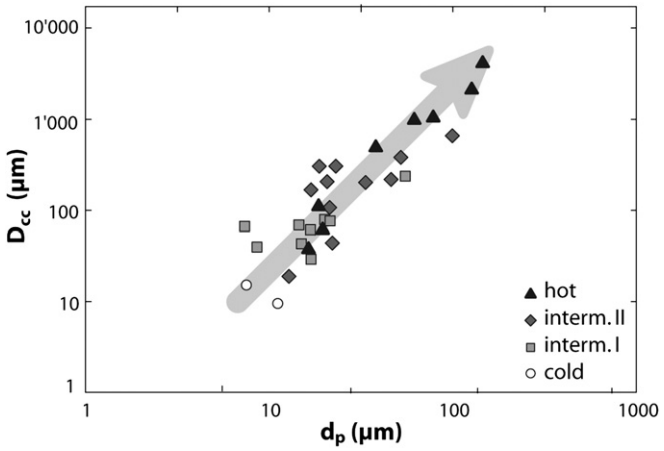

Fig. 11. Coupled grain coarsening of calcite grains of the matrix and second phases. The larger the matrix grain size D_{cc}, the larger the second-phase grain size d_p. For higher temperature samples, d_p generally is larger than for lower temperature samples suggesting an enhanced coupled grain coarsening with temperature. Note that despite their high peak metamorphic temperature, some samples have relatively small D_{cc} and d_p.

Solomatov et al. (2002) and El-Khozondar et al. (2006) by means of computed models and experimental studies by Ohuchi and Nakamura (2007a; 2007b). Further important information is the enhanced coupled grain coarsening with increasing temperature (Fig. 11). This behavior can be inferred from samples with similar f_p, which show small and larger sizes of d_p–D_{cc} at low and high temperatures, respectively. The reason for enhanced coupled grain coarsening is related to the increased growth kinetics of both second phases and matrix phase at higher temperature. Despite relatively high temperatures, some samples show lower D_{cc} and d_p values (*SB05-07.1*, *-07.2*, −07.4, Table 1) than those found in other samples with the same temperature history and identical mineralogy (*SB05-09.1* and *-09.2*, Table 1). Consequently, it can be concluded that grain growth kinetics alone is not the only parameter that affects the growth behavior of the second phases. In a microstructural point of view, the aforementioned 'hot' samples with small sized sp and D_{cc} are characterized by very low Z values and are situated on trend I. According to Figs. 8 and 9 and a correlation parameter $K > 1$, they are pinned by SPP, MPP and CPP regimes. Hence, they show a larger volume of the grain boundary network compared to the high Z samples. Mass transfer processes, particularly along grain boundaries, are responsible for the nutrient transport required during couple grain coarsening (e.g., Ardell, 1972; Alexander et al., 1994; Manohar et al., 1998). In this sense, transport- or surface-controlled processes are considered to be rate limiting affecting the nucleation and growth rates during metamorphic reactions. However, the interparticle distances between sp particles as well as their surface areas are smaller in the case of the low Z sample. Both points would favor a faster growth rate, which is not the case. We therefore assume, that the rate-limiting parameter is related to the larger grain boundary volume of the low Z samples. The latter requires a larger amount of source material to saturate the grain boundary network, while for high Z samples less material is required, delivering sufficient nutrient supply at grain surface of the second phases and promoting therefore a faster growth (Figs. 8 and 11). A small matrix grain boundary network, i.e., large calcite grains, will benefit from the coarsening of second phases as it is illustrated in Fig. 12. Coarsening of second phases will lead again to an unpinning of matrix grain boundaries, because under closed system conditions, some second phases have to grow at the expense of others, resulting at least in shrinkage and eventually in disappearance of some. At these locations, the calcite grain

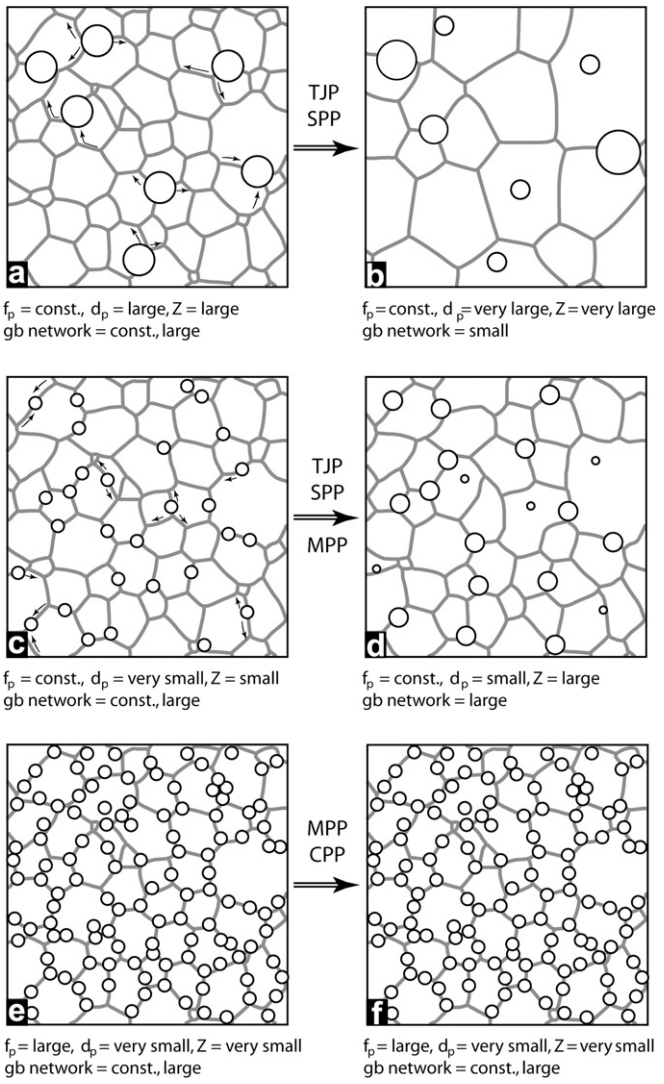

Fig. 12. Schematic summary of different types of coupled grain coarsening. For a small number of sp particles (white circles) with large grain sizes d_p (a), only few matrix grain boundaries (gray) are pinned, while the rest of them are able to migrate. This leads to a reduction of the bulk grain boundary network, which favors the coarsening of sp particles (b). In this case, coupled grain coarsening occurs, which is matrix controlled and affected by second-phase and/or triple junction pinning. For an equal second-phase volume fraction f_p compared to (a) but smaller sp particle sizes (c), i.e., higher number of particles, more matrix grain boundaries are pinned. With progressive coarsening, grain boundary migration of the matrix phase is reduced resulting in a small grain size and therefore a still relatively large bulk grain boundary network (d). Consequently, coarsening of second phases is slower. For the same sp-particles sizes as in (c) but with higher f_p (e) all matrix grain boundaries are pinned. Grain size of the matrix grains can only increase when the second phases grow requiring coupled grain coarsening, which is limited by the second phases (f).

boundaries are affected by smaller dragging forces, allowing the calcite grains to grow again until becoming pinned by the next second-phase grain. As a consequence of this interplay, matrix grain growth due to coupled grain coarsening is still possible even for grain boundaries pinned by the different pinning regimes.

The reactivation of grain boundary migration for pinned matrix grain boundaries will occur for samples on trend II as long as the intrinsic driving forces of the matrix grains are high enough, and for samples of trend I as long as they are again pinned by too many sp particles. In this way, trend I is limited by second-phase coarsening, while trend II is limited by matrix growth.

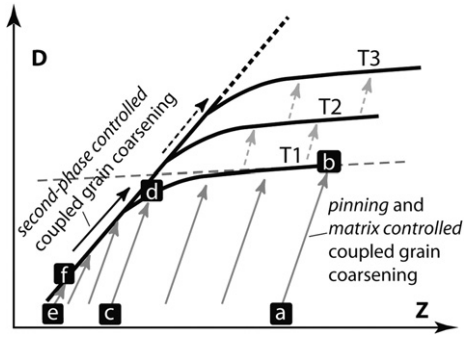

Fig. 13. Schematic model of the microstructural evolution of matrix grain size in dependence of Z and different temperatures. Matrix grain size D evolves according to the two trends dependent on the Zener value Z. For higher temperatures (e.g., T3) both trends are shifted to higher D and Z compared to lower temperatures (e.g., T1). The shift to higher Z values results from coarsening of second phases as is explained in Fig. 12. Letters (a) to (f) symbolize the possible microstructures given in Fig. 12 for the different situations. Gray arrows indicate pinning and matrix controlled growth paths for matrix grains during coupled grain coarsening, while the black arrow represents a second-phase controlled coupled grain coarsening path for matrix grains. Note that for higher T the change of trend occurs at higher Z (lower f_p) as larger matrix grains with longer grain boundaries are more likely to come into influence of MPP at lower f_p values.

Considering different temperatures and their related evolution, we assume that pinning regimes and the process of coupled grain coarsening described above can occur at every temperature (Figs. 12 and 13). Evidence for this assumption is given by the 'intermediate I' and 'II', and 'hot' samples, which all contain samples that are located on trend I. As discussed, the transition from trend I to II is related to a change in pinning regimes, and is documented in our database for the intermediate samples only. We believe, however, that a similar branching off of trend II must also occur for the hot samples, but at clearly larger grain sizes as is the case for the intermediate samples (Fig. 13). For a given f_p, d_p will increase resulting in a larger Z, which in turn allows the calcite matrix to grow to larger sizes. Starting with an original micritic microfabric with moderate to low second-phase contents Z will progressively shift toward higher values with increasing temperature. Due to this shift in Z, high D_{cc} for relatively low Z cannot be obtained, resulting in the empty domain in the upper left corner of the Zener diagram (field I in Fig. 6). A schematic model for this microstructural evolution is presented in Fig. 13, which might be of general validity for contact metamorphic polymineralic rocks containing a dominant matrix phase. The fact that our hot samples display no data points at high Z is most likely due to a starting material with insufficient degree of purity.

6. Conclusion

In contrast to previous studies, which mostly restricted the Zener parameter to polymineralic aggregates either with relatively low contents (e.g., Miodownik, 2005) or large contents (e.g., Alexander et al., 1994) of second phases, our investigation demonstrates that the Zener parameter has relevance for both systems allowing microstructural discriminations for a variety of sp volume fractions ranging from nearly pure (f_p: 0.001) up highly impure (f_p up to 0.5) polymineralic systems. Within this considerable range, the Zener diagram visualizes two pronounced microstructural trends, which result from two end member processes: (i) For moderate to high Z values, the grain boundary mobility is affected by the grain growth kinetics of the matrix phase and the retarding forces imposed by the second phases or additional influences like triple junctions. (ii) In the case of low Z values, the matrix grains are completely immobilized by the large amount and/or large size of second phases. Hence, grain coarsening of the aggregate is only possible, when the second phases are capable of coarsening themselves, giving the matrix phase new space to grow as well. In this coupled coarsening, the growth kinetics of the second-phase mineralogy is rate limiting. Both end member processes are the result of the interplay of different parameters, such as the size, volume fraction and distribution of the second phases and their changes as function of time and temperature. Only the combined analysis of different geometric parameters of a microstructure and the integration of experimental studies, helps to unravel the individual contribution of each parameter to the evolution of a polymineralic microstructure that underwent grain coarsening under static conditions.

Our dataset furthermore suggests that the physical interactions shown between different growing phases allow the use of geometrical relationships also in the case of metamorphic systems including net transfer reactions. We demonstrated the complex interactions between matrix phases and second-phase mineralogy during coupled grain coarsening and the different pinning regimes involved. The understanding of the different regimes of pinning and the related overgrowth behavior could be a key for interpreting the sequential evolution of metamorphic microstructures and the interplay with deformation. The presented relationships will also give the possibility to investigate grain size evolution in more complex rocks. Such data are necessary for all grain size sensitive processes in the Earth's crust, where there is deformation or mass transport. For example, matrix grain sizes can be kept small even at elevated temperatures owing to multiparticle or clustered particle pinning, while the corresponding grain sizes of purer domains will be large. During the onset of deformation, strain may localize in the fine-grained domains owing to the activation of grain-size sensitive mechanisms and the reduced rock flow stresses during the activation of these deformation mechanisms. Future work should include the role of time on the different processes and combine the presented geometrical relations with petrological observations.

Acknowledgments

Financial support by SNF grant no. 200021-109369 for the SEM at the Institute of Geological Sciences (University of Bern) as well as financial support by SNF by project grants numbers 200021-105316 and 200020-117514 is gratefully acknowledged. Special thanks goes to S. Brechbühl and V. Jakob for the outstanding preparation of the EBSD samples. T. Blenkinsop, R. Joesten and an anonymous reviewer are acknowledged for their interest in the obtained research results and the constructive reviews, which helped to improve the manuscript significantly.

References

Adams, B.L., Wright, S.I., Kunze, K., 1993. Orientation imaging - the emergence of a new microscopy. Metallurgical and Materials Transactions A 24, 819–831.
Alexander, K.B., Becher, P.F., Waters, S.B., Bleier, A., 1994. Grain growth kinetics in alumina-zirconia (CeZTA) composites. Journal of the American Ceramic Society 77 (4), 939–946.
Ardell, A.J., 1972. Cumulative distribution functions associated with particle coarsening processes. Metallography 5 (3), 285–294.
Barrett, S.D., 2008. Image SXM.
Berger, A., Brodhag, S.H., Herwegh, M., 2010. Reaction-induced nucleation and growth v. grain coarsening in contact metamorphic, impure carbonates. Journal of Metamorphic Geology 28, 809–824.
Berger, A., Herwegh, M., 2004. Grain coarsening in contact metamorphic carbonates: effects of second-phase particles, fluid flow and thermal perturbations. Journal of Metamorphic Geology 22, 459–474.
Bestmann, M., Prior, D.J., 2003. Intragranular dynamic recrystallization in naturally deformed calcite marbles: diffusion accommodated grain boundary sliding as a result of subgrain rotation recrystallization. Journal of Structural Geology 25, 1597–1613.
Brack, P., 1983. Multiple intrusions - examples from the Adamello batholith (Italy) and their significance on the mechanism of intrusions. Memorie della Società Geologica Italiana 26, 145–157.

Brodhag, S.H., Herwegh, M., 2009. Experimental insights on static grain growth in a two-phase system (norcamphor - glass beads). Contributions to Mineralogy and Petrology 160 (2), 219–238.
Bucher, K., Frey, M., 1994. Petrogenesis of Metamorphic Rocks. Springer, Berlin Heidelberg, p. 318.
Bunge, J., 1982. Inhomogeneous textures. Zeitschrift für Metallkunde 73 (8), 483–488.
Burhan, N., Ferry, M., 2006. Changes in grain size distribution of a submicron grained Al-Sc alloy during high temperature annealing. Materials Science Forum 519–521, 1617–1623.
Callegari, E., Dal Piaz, G., Gatto, G.O., 1998. Carta Geologica del Gruppo Adamello-Presanella SILCA Firenze.
Cui, X., Nabelek, P., Liu, M., 2003. Reactive flow of mixed CO_2–H_2O fluid and progress of calc-silicate reactions in contact metamorphic aureoles: insights from two-dimensional numerical modelling. Journal of Metamorphic Geology 21, 663–684.
Ebert, A., Herwegh, M., Pfiffern, A., 2007a. Cooling induced strain localization in carbonate mylonites within a large-scale shear zone (Glarus thrust, Switzerland). Journal of Structural Geology 29 (7), 1164–1184.
Ebert, A., Herwegh, M., Berger, A., 2008. Grain coarsening maps for polymineralic carbonate mylonites: a calibration based on data from different Helvetic nappes (Switzerland). Tectonophysics 457 (3–4), 128–142.
Ebert, A., Herwegh, M., Evans, B., Pfiffner, O.A., Austin, N., Vennemann, T., 2007b. Microfabrics in carbonate mylonites along a large-scale shear zone (Helvetic Alps). Tectonophysics 444, 1–26.
El-Khozondar, R., El-Khozondar, H., Gottstein, G., Rollet, A., 2006. Microstructural simulation of grain growth in two-phase polycrystalline materials. Egyptian Journal of Solids 29 (1), 35–47.
Evans, B., Renner, J., Hirth, G., 2001. A few remarks on the kinetics of static grain growth in rocks. International Journal of Earth Sciences 90, 88–103.
Ferry, M., Hamilton, N.E., Humphreys, F.J., 2005. Continuous and discontinuous grain coarsening in a fine-grained particle-containing Al–Sc alloy. Acta Materialia 53, 1097–1109.
Freund, D., Rybacki, E., Dresen, G., 2001. Effect of impurities on grain growth in synthetic calcite aggregates. Physics and Chemistry of Minerals 28, 737–745.
Gladman, T., 1966. On the theory of the effect of precipitate particles on grain growth in metals. Proceedings of the Royal Society of London. Series A, Mathematical and Physical Sciences 294, 298–309.
Gottstein, G., Molodov, D.A., Shvindlerman, L.S., 2006. Kinematics, dynamics, and microstructural effects of grain boundary junctions. Journal of Materials Science 41, 7730–7740.
Hansmann, W., Oberli, F., 1991. Zircon inheritance in an igneous rock suite of the southern Adamello batholith (Italian Alps): implication for petrogenesis. Contributions to Mineralogy and Petrology 107, 501–518.
Hellman, P., Hillert, M., 1975. On the effect of second-phase particles on grain growth. Scandinavian Journal of Metallurgy 4, 211–219.
Herwegh, M., 2000. A new technique to automatically quantify microsturctures of finegrained carbonate mylonites: two-step etching combined with SEM imaging and image analysis. Journal of Structural Geology 22 (4), 391–400.
Herwegh, M., Berger, A., 2003. Differences in grain growth of calcite: a field-based modeling approach. Contributions of Mineralogy and Petrology 145, 600–611.
Herwegh, M., Berger, A., 2004. Deformation mechanisms in second-phase affected microstructures and their energy balance. Journal of Structural Geology 26, 1483–1498.
Herwegh, M., Berger, A., Ebert, A., 2005. Grain coarsening maps: a new tool to predict microfabric evolution of polymineralic rocks. Geology 33, 801–804.
Herwegh, M., Ebert, A., Berger, A., Brodhag, S.H., 2008. Discrimination of annealed and dynamic fabrics: Consequences for strain localization and deformation episodes of large-scale shear zones. Earth and Planetary Science Letters 276 (1–2), 52–61.
Herwegh, M., Kunze, K., 2002. The influence of nano-scale second-phase particles on deformation of fine grained calcite mylonites. Journal of Structural Geology 24, 1463–1478.
Joesten, R.L., 1983. Grain growth and grain-boundary diffusion in quartz from the Christmas Mountains (Texas) contact aureole. American Journal of Science 283 (A), 233–254.
Joesten, R.L., 1991. Kinetics of coarsening and diffusion controlled mineral growth. Reviews in Mineralogy 26, 507–582.
Kruhl, J.H., 2001. Crystallographic control on the development of foam textures in quartz, plagioclase and analogue material. International Journal of Earth Sciences 90, 104–117.
Manohar, P.A., Ferry, M., Chandra, T., 1998. Five decades of the Zener equation. Iron and Steel Institute of Japan International 38 (9), 913–924.
Mas, D.L., Crowley, P.D., 1996. The effect of second-phase particles on stable grain size in regionally metamorphosed polyphase calcite marbels. Journal of Metamorphic Geology 14, 155–162.
Miodownik, M.A., 2005. Grain boundary engineering with particles. Scripta Materialia 54, 993–997.
Nabelek, P.I., 2007. Fluid evolution and kinetics of metamorphic reactions in calc-silicate contact aureoles - From H_2O to CO_2 and back. Geology 35 (10), 927–930.
Nakamura, M., Yurimoto, H., Watson, E.B., 2005. Grain growth control of isotope exchange between rocks and fluids. Geology 33 (10), 829–832.
Ohuchi, T., Nakamura, M., 2007a. Grain growth in the forsterite-diopside system. Physics of the Earth and Planetary Interiors 160, 1–21.
Ohuchi, T., Nakamura, M., 2007b. Grain growth in the forsterite-diopside-water system. Physics of the Earth and Planetary Interiors 161, 281–304.
Olgaard, D.L., Evans, B., 1986. Effect of second-phase particles on grain growth in calcite. Journal of American Ceramic Society 69 (11), C-272–C-277.
Pande, C.S., Masumura, R.A., 2005. Grain growth and deformation in nanocrystalline materials. Materials Science and Engineering A 409, 125–130.
Petrishcheva, E., Renner, J., 2005. Two-dimensional analysis of pore drag and drop. Acta Materialia 53, 2793–2803.
Piazolo, S., Bestmann, M., Prior, D.J., Spiers, C.J., 2006. Temperature dependent grain boundary migration in deformed-then-annealed material: observations from experimentally deformed synthetic rocksalt. Tectonophysics 427, 55–71.
Piazolo, S., Prior, D.J., Holness, M.D., 2005. The use of combined cathodoluminescence and EBSD analysis: a case study investigating grain boundary migration mechanisms in quartz. Journal of Microscopy 217 (2), 152–161.
Poirier, J.-P., Guillopé, M., 1979. Deformation induced recrystallization of minerals. Bulletin de Mineralogie 102 (2–3), 67–74.
Prior, D.J., Trimby, P.W., Weber, U.D., Dingley, D.J., 1996. Orientation contrast imaging of microstructures in rocks using forescatter detectors in the scanning electron microscope. Mineralogical Magazine 60 (403), 859–869.
Renner, J., Evans, B., Hirth, G., 2002. Grain growth and inclusion formation in partially molten carbonate rocks. Contributions to Mineralogy and Petrology 142 (5), 501–514.
Riege, S.P., Thompson, C.V., Frost, H.J., 1999. Simulation of the influence of particles on grain structure evolution in two-dimensional systems and thin films. Acta Materialia 47 (6), 1879–1887.
Riklin, K., 1983. Contact metamorphism of the permian 'red sandstone' in the Adamello area. Memorie della Società Geologica Italiana 26, 159–169.
Schmid, J., 1997. The Genesis of White Marble: Geological Causes and Archeological Applications. In: Institute of Geological Sciences, PhD. University of Bern, Bern, p. 156.
Shvindlerman, L.S., Gottstein, G., 2005. Cornerstones of grain structure evolution and stability: vacancies, boundaries, triple junctions. Journal of Materials Sciences 40, 819–839.
Simpson, C.J., Aust, K.T., Winegard, W.C., 1971. The four stages of grain growth. Metallurgical Transactions 2, 987–991.
Smith, C.S., 1948. Grains, phases, and interfaces: an interpretation of microstructure. Transactions of the American Institute of Mining, Metallurgical, and Petroleum Engineers 175, 15–51.
Solomatov, V.S., El-Khozondar, R., Tikare, V., 2002. Grain size in the lower mantle: constraints from numerical modeling of grain growth in two-phase systems. Physics of the Earth and Planetary Interiors 129, 265–282.
Song, W.J., Ree, J.H., 2007. Effect of mica on the grain size of dynamically recrystallized quartz in a quartz-muscovite mylonite. Journal of Structural Geology 29 (12), 1872–1881.
Stöckhert, B., Duyster, J., 1999. Discontinuous grain growth in recrystallized vein quartz - implications for grain boundary structure, grain boundary mobility, crystallographic preferred orientation, and stress history. Journal of Structural Geology 21, 1477–1490.
Weygand, D., Bréchet, Y., Lépinoux, J., 2000. Inhibition of grain growth by particle distribution: effect of spatial heterogeneities and of particle strength dispersion. Materials Science and Engineering A292, 34–39.
Wheeler, J., Jiang, Z., Prior, D.J., Tullis, J., Drury, M.R., Trimby, P.W., 2003. From geometry to dynamics of microstructure: using boundary lengths to quantify boundary misorientations and anisotropy. Tectonophysics 376, 19–35.
Zheng, Y.G., Lu, C., Mai, Y.-W., Zhang, H.W., Chen, Z., 2006. Model-based simulation of normal grain growth in a two-phase nanostructured system. Science and Technology of Advanced Materials 7, 812–818.